ACS Photonics

pubs.acs.org/journal/apchd5

Article

Spectrally Resolved Nonlinear Optical Properties of Doped *Versus* Undoped Quasi-2D Semiconductor Nanocrystals: Copper and Silver Doping Provokes Strong Nonlinearity in Colloidal CdSe Nanoplatelets

Katarzyna C. Nawrot,[#] Manoj Sharma,[#] Bartłomiej Cichy, Ashma Sharma, Savas Delikanli, Marek Samoć, Hilmi Volkan Demir,* and Marcin Nyk*

Cite This: *ACS Photonics* 2022, 9, 256−267

Read Online

ACCESS | Metrics & More | Article Recommendations | Supporting Information

ABSTRACT: Nonlinear optical processes are crucial for emerging applications including multiphoton-excited fluorescence microscopy and optical power limiting. Therefore, searching for materials of high multiphoton absorption cross sections is essential for the development of these techniques. We present synthesis of 4.5 monolayer CdSe nanoplatelets (NPLs) doped with silver and copper ions along with the evaluation of their two-photon absorption (TPA) and three-photon absorption (3PA) cross sections. Doping significantly increases the TPA cross section of each NPL sample, which reaches up to 1.33×10^7 GM for the most absorbing copper-doped ones. We also detected 1−2 orders of magnitude-enhanced 3PA cross sections for the doped NPLs in comparison with their undoped counterparts. As TPA and 3PA peaks appear, in the first and the second biological transmission windows, respectively, doped NPLs are promising candidates for multiphoton fluorescence microscopy as bioimaging agents. Moreover, the strong nonlinear response suggests application as active optoelectronic materials in optical sensors.

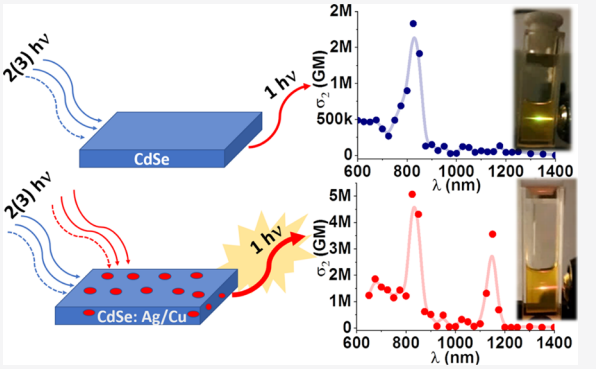

KEYWORDS: *quantum nanoplatelets, quantum dots, two-photon absorption, nonlinear optics, multiphoton fluorescence*

Downloaded via BILKENT UNIV on January 24, 2022 at 06:13:59 (UTC).
See https://pubs.acs.org/sharingguidelines for options on how to legitimately share published articles.

INTRODUCTION

Investigations of nonlinear optical (NLO) properties, and in particular nonlinear absorption of nanomaterials, have become an important issue for the development of numerous NLO-based techniques used in different fields, such as multiphoton-excited fluorescence microscopy in medical diagnosis[1,2] or optical power limiting in laser-based technologies.[3] For such applications, semiconductor nanoparticles offer several advantages over other materials, for example, their high luminescence brightness and stability against photobleaching exceed those of organic dyes. Furthermore, semiconductor nanoparticles exhibit narrow, often symmetric bands in photoluminescence (PL) spectra and may be excited within a broad wavelength range.[1] The tuning of their optical properties by the size effect allows one to obtain the maximum of two-photon absorption (TPA) or in some cases even three-photon absorption (3PA) in the range of the so-called "biological transmission windows", which makes them useful for biological applications. Moreover, in contrast to standard organic dyes which display TPA cross sections below 1000 GM,[4] but mostly even below 50 GM,[5] 0D spherical quantum dots (QDs) often reach the magnitudes of 10^3 to 10^5 GM.[6−11]

Even higher TPA cross sections have been reported for 1D and 2D semiconductor nanoparticles. Depending on the dimensions, both responsible for the quantum confinement and the lateral ones, the values for quantum rods may be of 10^5 GM order of magnitude,[10,12] while for semiconductor nanoplatelets (NPLs), they may reach up to 10^7 GM for the larger and thicker particles.[10] Naturally, comparisons of TPA merit of various materials need to consider these values in conjunction with the size of the system, for example, by calculating weight-normalized cross sections,[13] as will be done later in this paper.

However, increasing the size of nanoparticles not only increases their TPA cross section but also limits applications in which smaller sizes are required and changes their optical

Received: September 22, 2021
Published: January 4, 2022

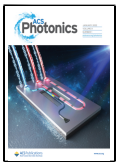

© 2022 The Authors. Published by American Chemical Society

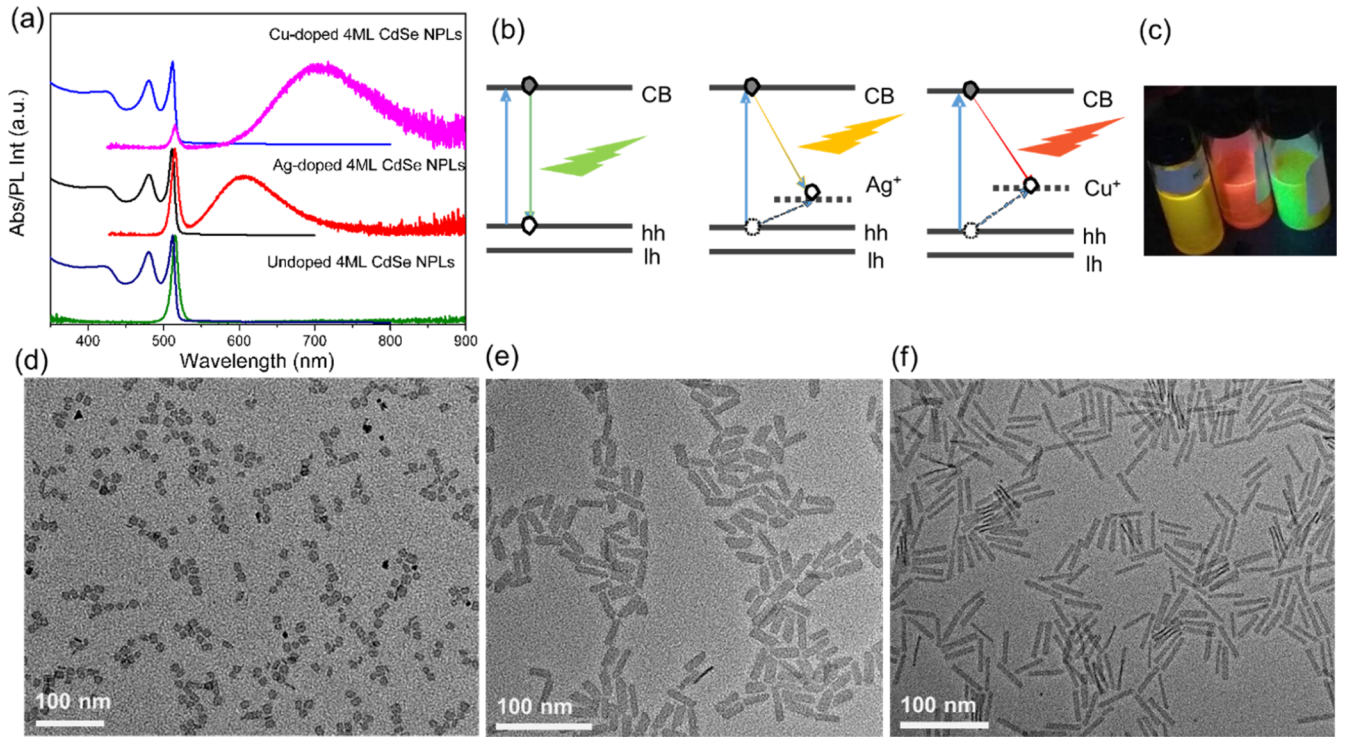

Figure 1. Absorption and PL spectra upon (one-photon) excitation at 400 nm of undoped, 0.4%-Ag-doped, and 0.5% Cu-doped 4.5 ML CdSe NPLs, (b) energy-band diagram and recombination sketch of undoped and (Cu/Ag)-doped CdSe NPLs (energetic position of the Ag state is estimated from ref 23) to be 0.34 eV above the bulk valence band and by comparing the emission peak position, the energetic position of the Cu level is estimated to be 0.27 eV above the bulk valence band, (c) color images of doped and undoped CdSe NPLs under 365 nm (UV lamp) excitation, and (d–f) TEM micrographs of undoped, Ag-doped, and Cu-doped CdSe NPLs, respectively.

response. For instance, 5.5 monolayer (ML)-thick CdSe NPLs with 82 nm × 22 nm lateral dimensions exhibit almost 40 times higher TPA cross section than 4.5 ML-thick CdSe NPLs with 26 nm × 13 nm lateral dimensions; however, their volume is almost seven times larger[10] and their first exciton peak as well as PL maximum is red-shifted by about 40 nm.[14]

Semiconductor nanoparticle properties can also be modified without changing their size. So far, many reports have been presented on doping nanocrystals, in a wide range of shapes and sizes, in order to tune their optical, magnetic, and electronic characteristics. For instance, Vlaskin *et al.*[15] introduced manganese impurity into ZnSe nanocrystals in order to enhance high-temperature dual emission. Moreover, CdSe QDs were doped with silver ions which increased the efficiency of QD-sensitized photovoltaic cells.[16] Furthermore, we have prepared copper-doped CdSe NPLs with extended quantum yields (QYs) as promising candidates for luminescent solar concentrators[17−19] and developed a light-emitting diode based on the material.[20] Manganese-doped ZnS QDs were also investigated in terms of their TPA cross section.[21]

However, up to date, the literature provides no information about NLO properties of 2D colloidal semiconductor NPLs doped with metal ions. This work contributes to filling this gap in knowledge of NLO properties of nanosystems, presenting TPA and 3PA absorption cross section spectra in a wide range of wavelengths for 4.5 ML CdSe NPLs doped with silver and copper ions.

EXPERIMENTAL SECTION

Chemicals. Cadmium nitrate tetrahydrate, sodium myristate, technical-grade 1-octadecene (ODE), selenium, cadmium acetate dihydrate, copper (II) acetate, silver acetate, trioctylphosphine (TOP), oleylamine, and technical-grade oleic acid (OA) were purchased from Sigma-Aldrich. Methanol, ethanol, acetone, and hexane were purchased from Merck Millipore.

Synthesis of Undoped and Cu- and Ag-Doped CdSe NPLs. Copper- and silver-doped colloidal CdSe NPLs were synthesized by following our previously published recipe with a few modifications.[17,18] In a three-neck flask, a mixture of 340 mg of cadmium myristate, 24 mg of Se, and 30 mL of ODE was degassed at 95 °C for 1 h. Then, the temperature of the reaction was adjusted to 240 °C and the atmosphere was switched to argon. A known amount of the Cu/Ag precursor was added at 190 °C and the solution was cooled down to 90 °C with a water bath. The solution was then degassed for a few minutes. Furthermore, the temperature of solution was set at 240 °C and shifted to argon at 100 °C. As the temperature reached 130 °C, 120 mg of cadmium acetate dihydrate was added in the powder form and the temperature was increased up to 240 °C where the reaction occurred for 10 min. Thereafter, it was terminated by adding 1 mL of OA followed by immediate cooling of the solution with a water bath. To get the final NPLs, the solution was centrifuged at 6000 rpm for 5 min. Then, ethanol was added to the supernatant and again centrifuged at 6000 rpm for 5 min. The final precipitates were suspended in hexane. The TOP/Cu and TOP/Ag ratio of 50 has been used for the preparation of the dopant precursor. The preparation of the dopant precursor was already given in our previous paper.[18]

The NLO measurements of NPLs were carried out as described previously (*e.g.*, ref 11), with some modifications.

https://doi.org/10.1021/acsphotonics.1c01456
ACS Photonics 2022, 9, 256−267

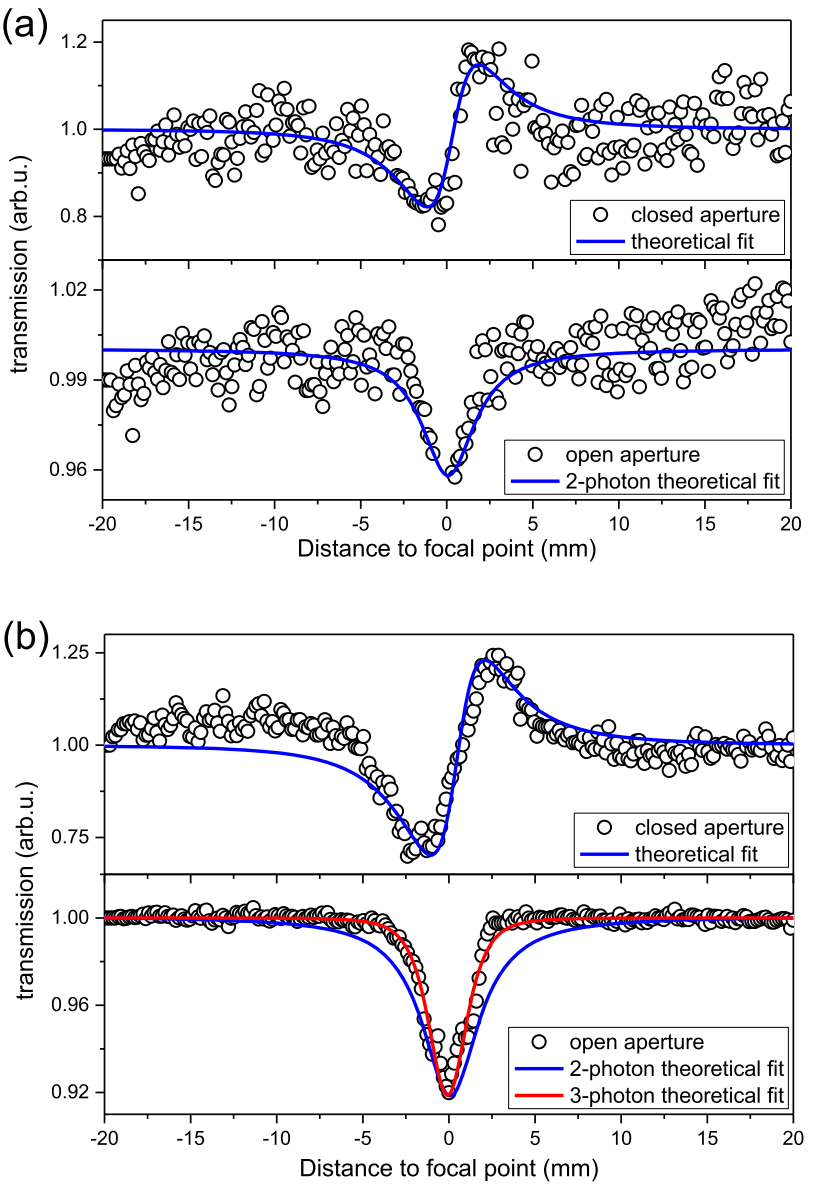

Figure 2. Representative open- and closed-aperture *Z*-scans and the theoretical fits for 0.5% Cu-doped 4.5 ML NPLs at (a) 850 and (b) 1225 nm. Data for the remaining samples are presented in the Supporting Information.

The wavelength-dependent NLO properties of the undoped, Ag-doped, and Cu-doped NPLs were studied with the open- and closed-aperture *Z*-scan technique using a laser system comprising a Quantronix Integra-C Ti:sapphire regenerative amplifier producing ∼130 fs, 800 nm pulses of 1 mJ energy per pulse at 1 kHz repetition rate and a Quantronix Palitra-FS optical parametric amplifier capable of delivering wavelengths between 500 and 1500 nm. In order to limit the data noise, a dedicated I/O card (National Instruments PCI-6143) with simultaneous sampling synchronized with the laser pulses was used to detect individual open- and closed-aperture signals together with the corresponding reference signal; thus, normalizing the signals by dividing them by the reference was enabled. For more details on how the calculations of NLO properties from raw open- and closed-aperture *Z*-scans were performed, see the Supporting Information. The UV−vis absorption spectra were measured using a JASCO V670 spectrophotometer. For the fluorescence measurements, the samples were excited using light of 400 nm wavelength and the emission spectra were detected with a Hitachi F-4500 spectrofluorometer. Absolute QYs of the synthesized samples were measured using the de Mello method.[22] The system is composed of a spectrometer (Ocean Optics Maya 2000), an integrating sphere (Hamamatsu), and a monochromator with an integrated xenon lamp. The excitation wavelength was set to 400 nm for these measurements. A Thermo X series II ICP−MS spectrometer was used to perform the elemental analysis.

Fast time-resolved PL spectra in the regime of both single- (400 nm) and two-photon (800 nm) excitation were measured using a streak camera. The setup used for the measurements consisted of a Coherent Libra-S all-in-one ultrafast oscillator and a regenerative amplifier system with a pulse duration of <100 fs at a 1 kHz repetition rate and a Coherent OperA-Solo optical parametric amplifier. The excitation laser system was synchronized with a Hamamatsu C5677 streak camera with a time resolution of 14 ps.

https://doi.org/10.1021/acsphotonics.1c01456
ACS Photonics 2022, 9, 256−267

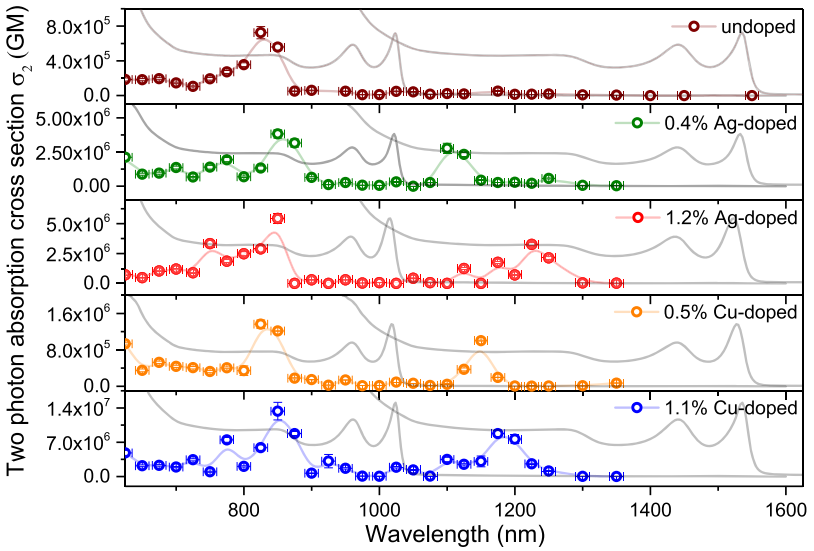

Figure 3. TPA cross-sectional spectra of all the examined samples. Light lines were added to guide the eye. One-photon absorption spectra in the function of doubled and tripled wavelength were added (gray lines) for comparison.

RESULTS AND DISCUSSION

For this study, we used two different doping concentrations both for Ag and Cu dopant ions in the same 4.5 ML CdSe NPL host with the doping concentrations estimated by ICP:MS measurements (Table S1) as 0.4 and 1.2% for Ag dopants and 0.5 and 1.1% for Cu dopants as the probes with average and maximum TPA cross sections, respectively (see Table S2 for the maximum TPA cross section of samples of different dopant concentrations). Previous reports with Cu and Ag doping in CdSe NPLs using partial cation exchange reactions have shown red shift of the emission spectrum with the increase in the doping level.[19,23,24] In these studies, we have used a high-temperature nucleation doping method for the synthesis of doped NPLs, and the level of doping for the studied samples is below 1.0%. This results in doping emission peaks at similar photon energies to those shown in our previous works.[19,25] Figure 1 shows the results for 0.4% Ag-doped and 0.5% Cu-doped 4.5 ML CdSe NPLs as compared to control undoped 4.5 ML CdSe NPLs. Figure 1a presents steady-state absorption and emission spectra of undoped and doped 4.5 ML CdSe NPLs. As compared to their undoped counterparts, Ag- and Cu-doped NPLs show the emergence of additional Stokes-shifted dopant-related emission along with typical excitonic emission at 514 nm. Ag-doped NPLs show the broadband Stokes-shifted emission at ∼600 nm, and Cu-doped NPLs show a similar broadband emission at ∼700 nm. Their absorption spectra are very similar to those of undoped 4.5 ML CdSe NPLs, showing typical e-hh and e-lh absorption transitions at 512 and 480 nm, respectively. The PL peak emission wavelength for the dopant-induced emission does not appear to red shift with variation in doping values as compared to previously reported partial cation-exchange reactions where a higher amount of doping leads to a huge red shift in the dopant-induced emission spectrum.[19,23,24] The PL emission spectra of different Ag- and Cu-doped CdSe NPLs used in the study are given in the Supporting Information (Figure S1). Figure 1b shows the energy band diagram of undoped and doped NPLs. Both Ag and Cu dopants show a very similar recombination mechanism. Both dopants act as hole traps, as the photoexcited holes are trapped by these localized dopant states, and recombination of delocalized electrons in the conduction band with these mid-gap trap states leads to Stokes-shifted dopant-induced emissions.[18,26] Figure 1c shows the typical images of doped and undoped NPLs under UV lamp excitation. Figure 1d–f shows the TEM micrographs for undoped and Ag- and Cu-doped NPLs. As seen from the images, the typical dimensions of undoped, Ag-doped, and Cu-doped CdSe NPLs are 12.88 × 10.22 nm^2, 27.25 × 7.69 nm^2, and 36.31 × 5.10 nm^2, respectively. Figures 2 and 3 show representative open-aperture and closed-aperture *Z*-scan measurement traces. The shapes of the graphs differ depending on the wavelength and the examined sample (for the remaining samples, see the Supporting Information and Figures S2 to S9).

The most pronounced nonlinear absorption was detected between 825 and 925 nm and, additionally, in the range between 1100 nm and 1225 nm, depending on the sample. We performed a closer examination of the graphs shapes (*cf.* ref 27) which suggested the occurrence of a TPA mechanism in the former, shorter wavelength range (Figure 2a) and a three-photon process in the latter one (Figure 2b). These findings are confirmed by the respective slope values in Figures S10 and S11 which present the dependence of the integral PL intensity as a function of the excitation laser beam power at wavelengths corresponding to maxima at multiphoton absorption spectra. Moreover, Figure S12 shows the plot of transmittance *versus* input intensity measured for 1225 nm for the 1.2% Ag-doped sample with theoretical dependences for TPA and 3PA presenting correspondence of the experimental data with the three-photon process.

To confirm the viability of the NPLs for use as two- and three-photon-excited luminescence markers, we measured the luminescence under NIR femtosecond laser excitation. The representative two- and three-photon-induced luminescence spectra of the investigated samples are shown in Figures S13 to S22 together with the corresponding photographs, where an experiment illustrates the formation of a bright two- and three-photon-excited PL spot produced by a focused beam from the femtosecond laser.

Figure 3 shows that the wavelength ranges of substantial values of TPA cross sections correspond roughly to those

https://doi.org/10.1021/acsphotonics.1c01456
ACS Photonics 2022, 9, 256−267

Table 1. Comparison of TPA Cross Sections of Doped and Undoped Colloidal 4.5 ML CdSe NPLs in Chloroform Determined Using the *Z*-Scan Technique

4.5 ML CdSe NPLs	area (nm^2)	wavelength (nm)	σ_2 (GM)	σ_2/M (GM·mol·g^{-1})	σ_2/V (GM·nm^{-3})	$\sigma_2 \times$ QY (GM)	reference
undoped	132	825	$7.25 \times 10^5 \pm 7.01 \times 10^4$	1.31	4.59×10^3	1.60×10^5	this work
Ag-doped (0.4%)	262	850	$3.82 \times 10^6 \pm 3.07 \times 10^5$	3.47	1.21×10^4	2.10×10^6	this work
Ag-doped (1.2%)	210	850	$5.44 \times 10^6 \pm 4.34 \times 10^5$	6.17	2.16×10^4	3.26×10^6	this work
Cu-doped (0.5%)	185	825	$1.36 \times 10^6 \pm 9.42 \times 10^4$	1.75	6.12×10^3	8.43×10^5	this work
Cu-doped (1.1%)	213	850	$1.33 \times 10^7 \pm 1.79 \times 10^6$	14.8	5.19×10^4	9.98×10^6	this work
undoped	500	800	1.30×10^6	0.62	2.17×10^3	- (up to 5.85×10^5)	10
undoped	621	800	1.73×10^6	0.66	2.32×10^3	- (up to 0.78×10^5)	10
undoped	128	800	9.22×10^4	0.17	6.00×10^2	- (up to 4.15×10^4)	10
undoped	338	800	1.40×10^6	0.99	3.45×10^3	- (up to 0.63×10^6)	10
undoped	253	800	4.40×10^5	0.41	1.27×10^3	- (up to 1.98×10^5)	10

predicted by doubling the wavelengths of OPA but are blue-shifted, which may be rationalized by considering that during simultaneous absorption of two photons, a biexciton may be formed whose energy exceeds that of an exciton (*cf.* ref 9 28 29,).

The maximum values of TPA cross sections vary depending on the sample with the highest value equal to 1.51×10^7 GM detected for 1.1% Cu-doped NPLs. It is worth noting that a much lower TPA cross section, although still significant, 7.25×10^5 GM, was found for undoped NPLs. The obtained values are presented in Table 1 along with those from the work previously reported. TPA cross sections of 4.5 ML CdSe NPLs presented in that work did not exceed 2×10^6 GM, despite modifying their lateral dimensions, similar to the result for undoped CdSe NPLs obtained here, confirming that doping with copper and silver ions strengthens the nonlinear absorption ability of the nanomaterial. This result is in line with the expectations, as the introduction of an intermediate state due to the presence of Ag or Cu ions should produce a resonance enhancement that may be an effective approach to increase TPA cross-sectional values of CdSe NPLs.[30,31] Clearly, these phenomena are not fully rationalized yet, but one can expect that doping can add more flexibility in tuning the 2D material properties.[32] For example, Li and Dagenais showed that quantum confinement of electrons in QDs and additional discrete energy levels within the band gap formed in InAs/GaAs QDs can function as intermediate states for additional sub-band gap photon absorption.[33] These authors concluded that the greatly broadened tailing density of states in the QD-made material strongly enhances both one-photon absorption current generation and TPA process by introducing the mid-gap intermediate states. Furthermore, Mn and Cu dopants were observed to enhance the TPA cross section of ZnSe QDs by approximately five times with respect to undoped counterparts.[30] This enhancement originates from the introduction of dopant ion states in doped QDs which leads to enhanced trap states due to the distortion in the crystal structure by the impurities as a result of doping.

Since the investigated nanoparticles differ in molar mass and possess different QYs, to compare their TPA merit, we calculated a molar mass-normalized merit factor σ_2/M as well as two-photon excitation action cross section $\sigma_2 \times$ QY which assesses the two-photon-induced luminescence brightness. Both factors are found to be the lowest for the undoped sample and the highest for 1.1% Cu-doped NPLs; however, the proportions between individual values change. The results are presented in Table 1.

As mentioned above, all samples display an additional peak in their nonlinear absorption spectra, with the absorption maximum between 1100 and 1225 nm. Although they are plotted in Figure 3 as "effective" values of σ_2 (corresponding to an experiment carried out at a certain light intensity, ~250 GW/cm^2 in our case), the dominant effect in that part of spectrum is 3PA. It is apparent because the absorption takes place at the wavelengths which are red-shifted relative to doubled wavelengths of OPA and is also confirmed by the *Z*-scan open-aperture trace shapes corresponding to a 3PA process (Figure 3). The corresponding σ_3 values recalculated from those data reach up to 4.11×10^{-74} $cm^6 \cdot s^2$ for 1.0% Cu-doped NPLs exceeding the value detected for the undoped sample, 4.06×10^{-76} $cm^6 \cdot s^2$, by 2 orders of magnitude. The enhancement is also similarly substantial when molar mass-normalized results are compared (4.58×10^{-80} $cm^6 \cdot s^2 \cdot mol \cdot g^{-1}$ and 7.34×10^{-81} $cm^6 \cdot s^2 \cdot g^{-1}$, respectively). These values also exceed molar mass-normalized 3PA merit factor equal to 1.36×10^{-82} $cm^6 \cdot s^2 \cdot g^{-1}$ calculated previously for CdSe QDs[9] (Table 2). We have also presented the nonlinear refraction of colloidal

Table 2. 3PA Cross Sections of Undoped, Ag-Doped, and Cu-Doped 4.5 ML CdSe NPLs in Colloidal Solutions

4.5 ML CdSe NPLs	wavelength (nm)	σ_3 ($cm^6 \cdot s^2$)	σ_3/M ($cm^6 \cdot s^2 \cdot mol \cdot g^{-1}$)
undoped	1025	4.06×10^{-76}	7.34×10^{-81}
Ag-doped (0.4%)	1100	2.24×10^{-74}	2.03×10^{-80}
Ag-doped (1.2%)	1225	1.22×10^{-74}	1.38×10^{-80}
Cu-doped (0.5%)	1150	5.55×10^{-75}	7.13×10^{-81}
Cu-doped (1.1%)	1175	4.11×10^{-74}	4.58×10^{-80}

CdSe NPLs calculated from the CA *Z*-scan in the form of the nonlinear refractive cross section σ_R spectra (Figure S23), as this single-nanoparticle-oriented parameter, defined by Balu *et al.*,[34] allows one for simple comparison with σ_2. The data contain large error margins, due to the fact that they are obtained from differences of the nonlinear refraction of solutions and of the pure solvent and do not show clear trends, except for possible anomalies close to nonlinear absorption peaks. The values are scattered from -1.26×10^7 refractive GM (RGM) to 3.39×10^7 RGM. The extrapolated n_2 is in the range of -9.95×10^{-17} to $3.03 \times 10^{-16} \frac{m^2}{W}$, as shown in Figure S24. The large scatter of the results is due to the fact that even at the relatively high concentration of NPLs in solution, the nonlinear refraction response of the samples is still mostly dominated by the solvent and the cuvette cell walls.

https://doi.org/10.1021/acsphotonics.1c01456
ACS Photonics 2022, 9, 256−267

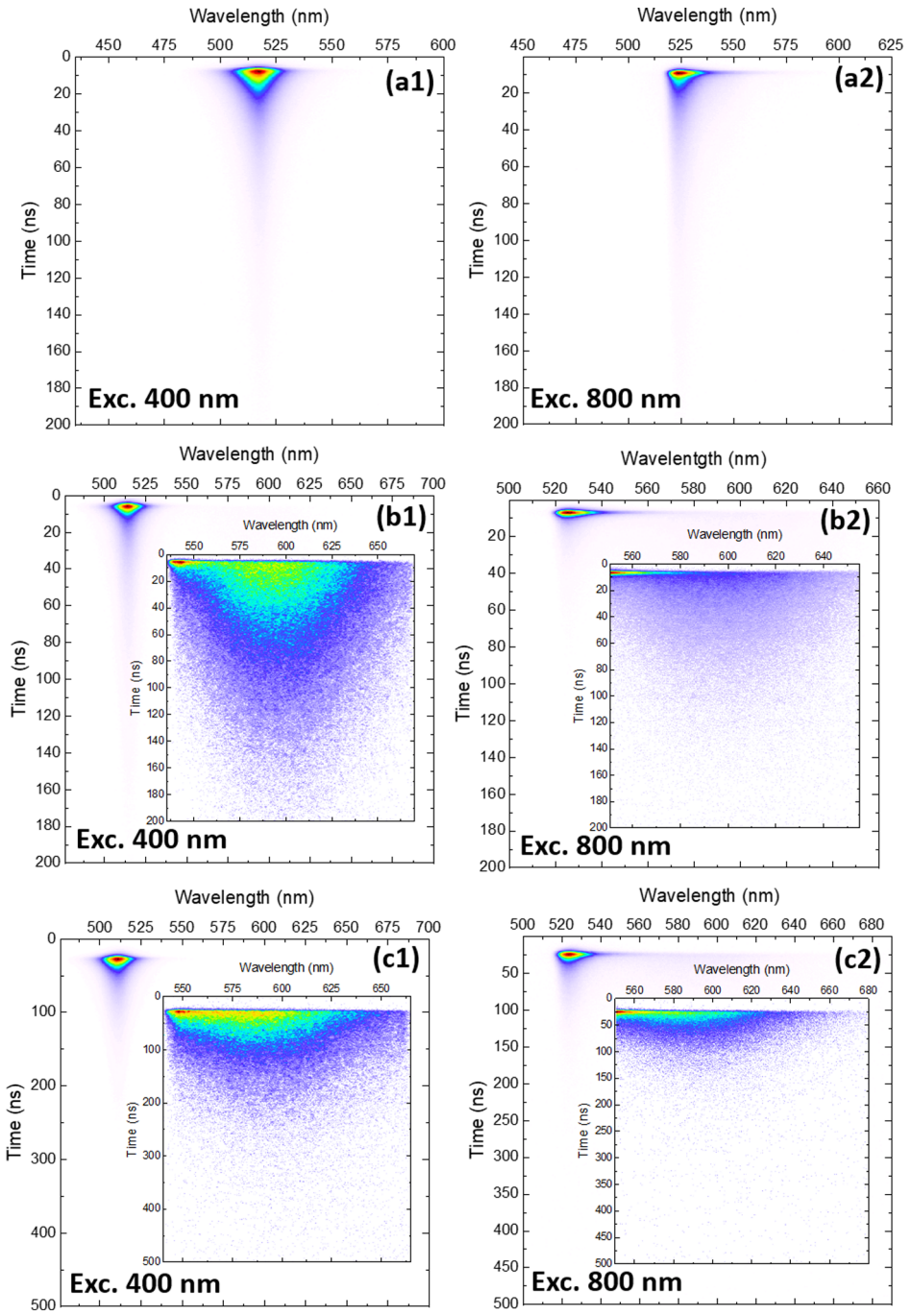

Figure 4. Streak camera images of (a) undoped CdSe NPLs and doped with (b) 0.4% and (c) 1.2% of silver (Ag). Notations a1−c1 refer to excitation in the single-photon regime, while a2−c2 refer to results obtained with two-photon excitation. Due to a strong difference in intensity between the excitonic and defect-related emission, the defect-related traces were placed in the form of insets.

Time-resolved PL spectroscopy of the samples was performed within the single- and two-photon excitation regime. The streak camera spectra taken for pristine CdSe and silver-doped (0.4 and 1.2% Ag) NPLs are shown in Figure 4. The results taken for the copper-doped (0.5 and 1.1% Cu) CdSe NPLs are presented in Figure 5.

According to the spectra taken for undoped CdSe NPLs within the single-photon excitation regime, it was found that the PL decays reveal two clear components (Figure 4a1). Regarding the undoped sample, the corresponding decay times were found as τ_1 = 4.5 ns ± 0.04 ns and τ_2 = 20.7 ns ± 0.3 ns (see Table 3). The amplitude-averaged lifetime τ was estimated as τ = 5.73 ± 0.07 ns. All decay curves with the fitting parameters may be found in Figure S34 and S35 of the Supporting Information section. In Figure S34, decay curves taken for the excitonic band are shown. Decay curves taken for the defect-related band have been shown in Figure S35. It is worth noting that multiexponential decays have also been reported for CdSe NPLs.[35,36] According to Kunneman,[37] the CdSe NPLs were found to exhibit blinking behavior analogous to QDs, which may help with interpretation of the time-resolved spectra.

The existence of the short component τ_1 in QDs is typically assigned to the internal charge disturbance that results from

https://doi.org/10.1021/acsphotonics.1c01456
ACS Photonics 2022, 9, 256−267

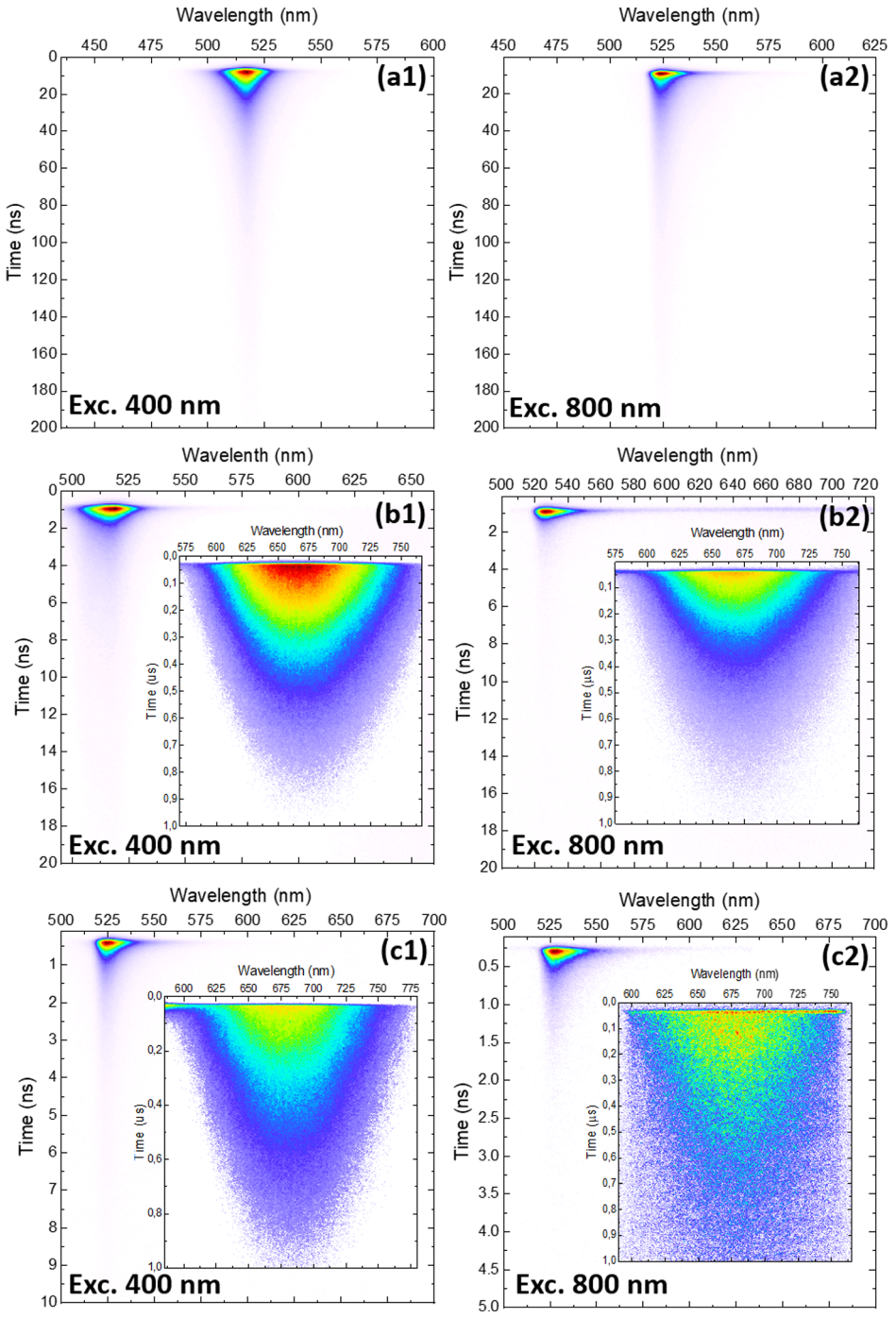

Figure 5. Streak camera images of (a) undoped CdSe NPLs and doped with (b) 0.5% and (c) 1.1% of copper (Cu). Notations a1−c1 refers to excitation in the single-photon regime, while a2−c2 refer to results obtained under two-photon excitation. Due to a strong difference in intensity between the excitonic and defect-related emission, the defect-related traces were placed in the form of insets.

charge trapping and the formation of charged excitons.[38−41] The charge disturbance is believed to be a result of efficient population of defect states in the first picoseconds after the excitation pulse. The fast component may therefore be identified with severe damping of the excitonic component by nonradiative relaxation channels induced by charged excitons.[38] Quenching of the X^0 relaxations by unbalanced holes/electrons is a natural consequence of substantial change in the relaxation probabilities.[42,43] Similar results were also reported by Kunneman *et al.*[37] For undoped NPLs, it is therefore likely that the charge imbalance is rather associated with the surface. Interlayer charge trapping may be properly omitted as the few-layer NPL is a strongly interacting system. The short decay component of undoped NPLs may be treated as the indicator of the density of trapping centers and their optical activity.

The situation looks slightly different for doped samples (Figure 4b1,c1). The sample doped with 0.4% of Ag exhibits notable shortening for both lifetime components, that is, τ_1 = 2.36 ns ± 0.01 ns and τ_2 = 17.96 ns ± 0.3 ns as well as τ = 2.63 ± 0.01 ns (Table 3). On the other hand, the CdSe:1.2% Ag sample revealed considerable elongation of the time constants

https://doi.org/10.1021/acsphotonics.1c01456
ACS Photonics 2022, 9, 256−267

Table 3. PL Band Maximum Positions and Decay Parameters Estimated from Streak Camera Spectra Obtained for One-Photon Excitation

sample	exciton band maximum	exciton band decay parameters					defect band maximum	defect band decay parameters τ (ns)
		τ_1 (ns)	τ_2 (ns)	A_1	A_2	τ (ns)		
undoped	517.48 nm	4.51 ± 0.04	20.77 ± 0.32	$3.364 \times 10^6 \pm 4.980 \times 10^4$	$2.736 \times 10^5 \pm 7.470 \times 10^3$	5.73 ± 0.07		
CdSe 0.4% Ag	513.70 nm	2.36 ± 0.01	17.96 ± 0.30	$1.262 \times 10^7 \pm 2.214 \times 10^5$	$2.256 \times 10^5 \pm 4.681 \times 10^3$	2.63 ± 0.01	594.03 nm	68.69 ± 6.62
CdSe 1.2% Ag	510.72 nm	6.56 ± 0.05	33.56 ± 0.71	$1.113 \times 10^8 \pm 3.506 \times 10^6$	$6.536 \times 10^5 \pm 2.745 \times 10^4$	6.71 ± 0.05	574.64 nm	68.09 ± 1.84
CdSe 0.5% Cu	517.02 nm	2.07 ± 0.03	$0.31 \pm 1 \times 10^{-3}$	$2.207 \times 10^5 \pm 5.418 \times 10^3$	$2.149 \times 10^7 \pm 4.222 \times 10^5$	0.32 ± 0.00	667.16 nm	260.07 ± 2.06
CdSe 1.1% Cu	525.17 nm	$0.10 \pm 1 \times 10^{-3}$	$0.51 \pm 9 \times 10^{-3}$	$1.257 \times 10^6 \pm 2.657 \times 10^4$	$9.915 \times 10^4 \pm 2.832 \times 10^3$	0.12 ± 0.00	676.12 nm	390.68 ± 8.91

up to τ_1 = 6.56 ns ± 0.05 ns and τ_2 = 33.56 ns ± 0.7 ns. This is also observed in a higher value of τ = 6.71 ± 0.05 ns. However, τ_1 has the dominant share for the value of τ. Observation of higher decay rates for the excitonic relaxations in the CdSe:0.4% Ag sample compared to undoped CdSe NPLs may be quite well-rationalized by the presence of additional defect states formed by silver atoms. Two separate radiative channels related to the X^0 exciton and defect E^{Ag} need to be considered.

As discussed, any charge imbalance (uncompensated holes or electrons) must imply severe changes in the excitonic transition probabilities. Depending on the ratio between trapping time and nonradiative rate constants, intense Auger relaxations or linear decreases in PL lifetime and intensity is expected.[44] Shortening and weakening of the excitonic component is therefore a natural consequence of charge trapping and is believed to be the best recognized mechanisms responsible for blinking in QDs.[38,45,46] The existence of broad PL emission for Ag-doped NPLs implies the occurrence of a second radiative channel, that is, defect-mediated transitions. Both these channels may in a first approximation be treated as uncorrelated; however, indication of a specific defect type mediating the relaxation is challenging and requires further theoretical studies. Different behaviors—due to different charge states—are expected from silver on cadmium antisites Ag_{Cd} and interstitial silver Ag_i. Elongation of the PL lifetime components for the CdSe:1.2% Ag sample may, however, be of different nature. It is important to note that defect formation energy is dependent on the chemical potential. Different defect types may be more probable for heavy silver-doped samples, that is, Ag_{Cd}^{-2} instead of Ag_{Cd}^{-}. The change in the charge state may have dramatic consequences on the defect-related relaxation rates. This change may also involve preferential formation of Ag_i^+ defects as the Ag doping in CdSe nanocrystals is shown to be a distribution of interstitial and substitutional sites.[47,48]

As heavy doping has a negative effect on X^0 transitions, a small amount of Ag doping in the CdSe host may enhance the excitonic emission by passivating the nonradiative channels. In our case, different amounts of Ag doping values in CdSe host NPLs can result in different distributions of interstitial *versus* substitutional doping sites. However, further analysis is required to understand the influence of different doping concentrations on host excitonic emission.

Considering the defect-related PL bands, no change in the radiative rates as a function of Ag ions concentration was noticed. Spectral shift of the defect band maximum from the excitonic band was estimated to be *ca.* 81 nm (0.32 eV). Both samples exhibit similar relaxation kinetics that follows the first-order decay law with characteristic lifetime parameters of τ = 68.69 ns ± 6.62 ns for the CdSe:0.4% Ag and τ = 68.09 ns ± 1.84 ns for the CdSe:1.2% Ag (Table 3). A slight temporal red shift was, however, observed for the defect-related band, which was 41.89 and 65.41 meV, for CdSe:0.4% Ag and CdSe:1.2% Ag (see Figure S25 of the Supporting Information), respectively.

This temporal red shift of the PL band maximum brings important physical premise according to the interplay between more than one defect types that are involved in the relaxation pathways. The defect transition energies may be related to isolated point defects and defect pairs. Concerning isolated point defects formed by silver(I) in the CdSe structure, it is justified to consider silver interstitials Ag_i and silver on

https://doi.org/10.1021/acsphotonics.1c01456
ACS Photonics 2022, 9, 256−267

Table 4. PL Band Maximum Positions and Decay Parameters Estimated from Streak Camera Spectra Obtained for Two-Photon Excitation

		exciton band decay parameters			
sample	exciton band maximum	τ_1 (ns)	τ_2 (ns)	defect band maximum	defect band decay parameters τ_1 (ns)
undoped	520.67 nm	1.68 ± 0.02	14.87 ± 0.21		
CdSe 0.4% Ag	525.17 nm	1.24 ± 0.01	11.16 ± 0.53	595.81 nm	41.92 ± 1.52
CdSe 1.2% Ag	523.83 nm	5.07 ± 0.07	35.17 ± 2.09	580.56 nm	52.95 ± 3.14
CdSe 0.5% Cu	526.83 nm	$0.17 \pm 2 \times 10^{-3}$	0.94 ± 0.05	664.94 nm	282.73 ± 20.62
CdSe 1.1% Cu	527.50 nm	$0.08 \pm 1 \times 10^{-3}$	0.42 ± 0.01	676.34 nm	384.88 ± 41.43

cadmium antisites Ag_{Cd}. The Ag_i (Ag_i^+) is seen to be a donor-like defect, whereas Ag_{Cd} (Ag_{Cd}^- or Ag_{Cd}^{2-}) is assumed to act as an acceptor. Due to limited valency for silver, it is reasonable to discuss the Ag^0 and Ag^+ states with characteristic transition energy $E(0/+)$. According to the Ag_{Cd} antisite, one may anticipate Ag_{Cd}^0 and Ag_{Cd}^- charge states associated with $E(-/0)$ transition energy. Depending on the formation energy, one may also anticipate higher-order defects involving charge-compensated pairs, that is, (Ag_{Cd}^- + Ag_i^+), (Ag_{Cd}^0 + Ag_i^0), or (V_{Cd}^{2-} + $2Ag_i^+$) formed with the assistance of cadmium vacancies. The existence of paired defects will be strongly dependent on the atomic chemical potential, changing strongly the overall ratio between various defect forms on concentration of silver in the CdSe samples. This may further have its reflection in the effective pathway for radiative relaxations with the excitonic channel. Another important feature is related to clear shifts in the position of the excitonic band maximum and the asymmetry of the excitonic band noted for samples excited in the two-photon regime (Figure 5a2−c2). This is well seen comparing single- and two-photon-excited spectra (Figure 5b1,b2,c1,c2). This asymmetry is represented as an elongated tail (*ca.* 160 meV) of the band toward lower energies and can be seen in Figures S26−S30 of the Supporting Information (Figures S31 and Figure S32 show temporal changes in the defect-related PL band). Measurements performed for various photon fluxes (Figure S33 for representative samples) proved that the excitonic asymmetry and shift of the PL band maximum results from the formation of the biexcitonic excitations. For lower photon fluxes, the excitonic band gains its symmetric character.

Results obtained for copper-doped samples are presented in Figure 5. Samples doped with copper reveal considerably stronger emission from the defect-related band (Figure 5b1,c1). The spectral shift between the excitonic maximum and the defect-related band maximum for copper-doped NPs was found to be *ca.* 150 nm (0.53 eV), which is about 0.21 eV more than what was found for silver-doped samples. Strong defect-mediated recombination for the CdSe:Cu NPs is clearly reflected in the excitonic relaxation channel. One may note that severe damping of excitonic relaxation is observed there (Table 3). The PL decay parameters for single-photon excitation were estimated for the CdSe:0.5% Cu and CdSe:1.1% Cu as τ_1 = 2.07 ns ± 0.03 ns and τ_2 = 0.31 ns ± 1×10^{-3} ns and τ_1 = 0.10 ns ± 1×10^{-3} ns and τ_2 = 0.51 ns ± 9×10^{-3} ns, respectively. This translates into the mean decay time values τ = 0.32 ns and τ = 0.12 ns, respectively, for CdSe:0.5% Cu and CdSe:1.1% Cu.

This may be well-rationalized considering intense capturing of excited charge by the defect centers, which is responsible for temporal charge disturbance in the NPLs as it was discussed above. The excitonic relaxation rates correlate with the concentration of copper in the CdSe structure. It may be seen that for the CdSe:1.1% Cu sample (Figure 5c1), the excitonic band also presents evident asymmetry related with a long tail in the range of lower energies even for single-photon excitation regime. Efficient biexcitonic systems are typically formed for 0.289 W of an average optical power at a 1 kHz repetition rate.

In contrast to silver, copper easily accepts Cu^{2+} oxidation states which are typically more preferred than Cu^+. This may have its reflection in the defect type that is formed in the CdSe structure. At the interstitial sites, copper may therefore be expected to form Cu_i^+ or Cu_i^{2+} states, whereas for cadmium antisites, it may form strong acceptor states. Relaxations through copper states may therefore be more preferred than through Cd−Se-related antibonding states. Concerning the defect-related PL band, one may also notice much longer decays than what was observed for silver-doped NPs. The CdSe:0.5% Cu sample is characterized by an exponential decay with a time parameter of τ_1 = 260.07 ns ± 2.06 ns and τ_1 = 390.68 ns ± 8.91 ns for the CdSe:1.1% Cu (Table 3). Small deviations of *ca.* 12 nm were observed in the defect band maximum and temporal red shift of the PL maximum (Figure S26) for the CdSe:0.5% Cu and CdSe:1.1% Cu samples. This may be well-rationalized by participation of different defect states that dominate at different Cu doping. These lifetimes are also matching with our previous reported lifetimes for Cu^+-doped CdSe NPLs.[18] For two-photon excitation, one may notice further shortening of the exciton decay parameters (Table 4). Excited-state relaxations are held here mainly with the participation of defect transitions (Figure 5b2,c2). Higher activity of Cu-related defects and higher polarizability of localized nonbonding charge associated with point defects may also explain higher values of σ_2 for the copper-doped nanoparticles. Similarly, as it was observed for silver-doped samples, the excitonic bands for two-photon excitation are characterized by strong asymmetry that is caused by biexcitonic system formation. The change in the relaxation rate for defect-related transitions is not unequivocal. The CdSe:0.5% Cu sample was characterized by a quite long decay time of τ_1 = 282.73 ns ± 20.62 ns, but the CdSe:1.1% Cu sample was characterized by a slightly shorter value of τ_1 = 384.88 ns ± 41.43 ns. No evident shift in the PL defect band maximum was also noted.

CONCLUSIONS

We have synthesized 4.5 ML CdSe NPLs, doped them with silver and copper ions, and characterized their optical properties, in particular, the multiphoton absorption cross sections. All the samples exhibit the maximum of nonlinear absorption in the wavelength range of 825−925 nm which we attribute to the TPA effect and an additional peak between 1100 and 1225 nm corresponding to the 3PA process. Doping the NPLs with Cu and Ag ions significantly increased σ_2, σ_3,

https://doi.org/10.1021/acsphotonics.1c01456
ACS Photonics 2022, 9, 256−267

and two-photon brightness, regardless of the nanoparticle molar masses. We conclude that with doping, it is possible to increase the TPA cross section of 4.5 ML CdSe colloidal NPLs at least up to 1.33×10^7 GM and their 3PA cross section to 4.11×10^{-74} $cm^6 \cdot s^2$. Such promising nonlinear absorption effects make them attractive materials for optical power limiters, for example, protecting sensitive sensors or eliminating laser work-related noises. Moreover, appearing in the range of biological transmission windows, in combination with high two-photon brightness of up to 1.13×10^7 GM, applications in multiphoton fluorescence microscopy, especially for biological samples, can be suggested.

To shed more light on the role of doping, we employed time-resolved spectroscopy, which revealed effective defect mediation in radiative relaxations for both silver- and copper-doped samples where PL decays lying in the range of *ca.* 50—to 400 ns were seen. This range of lifetime constants is favorable for fluorescence lifetime imaging and techniques utilizing Förster resonance energy transfer phenomena. For silver-doped nanoparticles, the PL decay lifetime was invariable in the function of silver concentration, which does not apply to copper-doped NPs for which the PL decay lifetime elongates for the heavily doped (1.1% of Cu) sample. A temporal shift of PL maximum for the defect band was observed for both samples. This effect was attributed to relaxations from more than one defect state or temporal charge rebalancing on the defect sites. The charge imbalance was also indicated as a major effect that is responsible for shortening of the excitonic relaxation constant. Two-photon-excited luminescence spectra showed significant asymmetry in the excitonic band. This asymmetry was related to band widening toward lower energies which was attributed to the efficient formation of biexcitonic excitations by the 800 nm laser beam. Severe shortening of the excitonic lifetime constants was observed for the two-photon excitation regime. Noticeable shortening was also observed for the defect-mediated transitions suggesting that stronger charge disturbance may be caused by two-photon excitations. The obtained results indicate that copper- and silver-doped CdSe NPLs are very efficient luminescence markers for both single- and multiphoton excitation. This is especially true for techniques requiring NIR excitation and two-band or two-color luminescence markers for special applications.

■ ASSOCIATED CONTENT

Supporting Information

The Supporting Information is available free of charge at https://pubs.acs.org/doi/10.1021/acsphotonics.1c01456.

Details on the NLO calculations, PL spectra *versus* concentrations, ICP—MS data, σ_2 versus concentration, open- and closed-aperture *Z*-scan traces, log—log plots of the PL intensity versus laser power, two photon-induced PL spectra, nonlinear refraction cross section σ_R, nonlinear refractive index n_2, and PL decay curves (PDF)

■ AUTHOR INFORMATION

Corresponding Authors

Hilmi Volkan Demir − *LUMINOUS Centre of Excellence for Semiconductor Lighting and Displays, The Photonics Institute (TPI), School of Electrical and Electronic Engineering, School of Physical and Mathematical Sciences, School of Materials Science and Engineering, Nanyang Technological University, Singapore 639798, Singapore; Department of Electrical and Electronics Engineering and Department of Physics, UNAM-Institute of Materials Science and Nanotechnology, Bilkent University, Ankara 06800, Turkey;* orcid.org/0000-0003-1793-112X; Email: hvdemir@ntu.edu.sg

Marcin Nyk − *Advanced Materials Engineering and Modelling Group, Faculty of Chemistry, Wroclaw University of Science and Technology, Wroclaw 50-370, Poland;* orcid.org/0000-0002-0329-4038; Email: marcin.nyk@pwr.edu.pl

Authors

Katarzyna C. Nawrot − *Advanced Materials Engineering and Modelling Group, Faculty of Chemistry, Wroclaw University of Science and Technology, Wroclaw 50-370, Poland*

Manoj Sharma − *LUMINOUS Centre of Excellence for Semiconductor Lighting and Displays, The Photonics Institute (TPI), School of Electrical and Electronic Engineering, School of Physical and Mathematical Sciences, School of Materials Science and Engineering, Nanyang Technological University, Singapore 639798, Singapore; ARC Centre of Excellence in Exciton Science, Department of Materials Science and Engineering, Monash University, Melbourne, Victoria 3800, Australia;* orcid.org/0000-0001-5215-9740

Bartłomiej Cichy − *Institute of Low Temperature and Structure Research, Polish Academy of Sciences, Wrocław 50-422, Poland;* orcid.org/0000-0001-9166-2728

Ashma Sharma − *LUMINOUS Centre of Excellence for Semiconductor Lighting and Displays, The Photonics Institute (TPI), School of Electrical and Electronic Engineering, School of Physical and Mathematical Sciences, School of Materials Science and Engineering, Nanyang Technological University, Singapore 639798, Singapore*

Savas Delikanli − *LUMINOUS Centre of Excellence for Semiconductor Lighting and Displays, The Photonics Institute (TPI), School of Electrical and Electronic Engineering, School of Physical and Mathematical Sciences, School of Materials Science and Engineering, Nanyang Technological University, Singapore 639798, Singapore; Department of Electrical and Electronics Engineering and Department of Physics, UNAM-Institute of Materials Science and Nanotechnology, Bilkent University, Ankara 06800, Turkey;* orcid.org/0000-0002-0613-8014

Marek Samoć − *Advanced Materials Engineering and Modelling Group, Faculty of Chemistry, Wroclaw University of Science and Technology, Wroclaw 50-370, Poland;* orcid.org/0000-0002-5404-2455

Complete contact information is available at: https://pubs.acs.org/10.1021/acsphotonics.1c01456

Author Contributions

#These authors contributed equally to the work.

Funding

This work has received financial support from the National Science Centre, Poland, under grant no. 2018/29/B/ST4/02172, the National Research Foundation of Singapore under program NRF-NRFI2016-08, and the Singapore Ministry of Education under grant MOE-RG62/20.

Notes

The authors declare no competing financial interest.

■ ACKNOWLEDGMENTS

K.C.N., M.S., and M.N. acknowledge support from the National Science Centre, Poland, under grant no. 2018/29/B/ST4/02172. This research is also supported by the National Research Foundation, Prime Minister's Office, Singapore, under its NRF Investigatorship Award program (NRF-NRFI2016-08) and the Ministry of Education Tier 1 grant (MOE-RG62/20). H.V.D. also gratefully acknowledges the support from TUBA. B.C. acknowledges support from a statutory activity subsidy for the Institute of Low Temperature and Structure Research of Polish Academy of Sciences.

■ REFERENCES

(1) Petryayeva, E.; Algar, W. R.; Medintz, I. L. Quantum Dots in Bioanalysis: A Review of Applications across Various Platforms for Fluorescence Spectroscopy and Imaging. *Appl. Spectrosc.* **2013**, *67*, 215−252.

(2) Meiling, T. T.; Cywiński, P. J.; Löhmannsröben, H.-G. Two-Photon Excitation Fluorescence Spectroscopy of Quantum Dots: Photophysical Properties and Application in Bioassays. *J. Phys. Chem. C* **2018**, *122*, 9641−9647.

(3) He, G. S.; Zheng, Q.; Yong, K.-T.; Ryasnyanskiy, A. I.; Prasad, P. N.; Urbas, A. Two-photon absorption based optical limiting and stabilization by using a CdTe quantum dot solution excited at optical communication wavelength of ∼1300nm. *Appl. Phys. Lett.* **2007**, *90*, 181108.

(4) Makarov, N. S.; Campo, J.; Hales, J. M.; Perry, J. W. Rapid, broadband two-photon-excited fluorescence spectroscopy and its application to red-emitting secondary reference compounds. *Opt. Mater. Express* **2011**, *1*, 551−563.

(5) Makarov, N. S.; Drobizhev, M.; Rebane, A. Two-photon absorption standards in the 550-1600 nm excitation wavelength range. *Opt. Express* **2008**, *16*, 4029−4047.

(6) Wawrzynczyk, D.; Szeremeta, J.; Samoc, M.; Nyk, M. Third-Order Nonlinear Optical Properties of Infrared Emitting PbS and PbSe Quantum Dots. *J. Phys. Chem. C* **2016**, *120*, 21939−21945.

(7) Szeremeta, J.; Nyk, M.; Wawrzynczyk, D.; Samoc, M. Wavelength dependence of nonlinear optical properties of colloidal CdS quantum dots. *Nanoscale* **2013**, *5*, 2388−2393.

(8) Achtstein, A. W.; Ballester, A.; Movilla, J. L.; Hennig, J.; Climente, J. I.; Prudnikau, A.; Antanovich, A.; Scott, R.; Artemyev, M. V.; Planelles, J.; Woggon, U. One- and Two-Photon Absorption in CdS Nanodots and Wires: The Role of Dimensionality in the One- and Two-Photon Luminescence Excitation Spectrum. *J. Phys. Chem. C* **2015**, *119*, 1260−1267.

(9) Nyk, M.; Wawrzynczyk, D.; Szeremeta, J.; Samoc, M. Spectrally resolved size-dependent third-order nonlinear optical properties of colloidal CdSe quantum dots. *Appl. Phys. Lett.* **2012**, *100*, 041102.

(10) Scott, R.; Achtstein, A. W.; Prudnikau, A.; Antanovich, A.; Christodoulou, S.; Moreels, I.; Artemyev, M.; Woggon, U. Two Photon Absorption in II-VI Semiconductors: The Influence of Dimensionality and Size. *Nano Lett.* **2015**, *15*, 4985−4992.

(11) Achtstein, A. W.; Hennig, J.; Prudnikau, A.; Artemyev, M. V.; Woggon, U. Linear and Two-Photon Absorption in Zero- and One-Dimensional CdS Nanocrystals: Influence of Size and Shape. *J. Phys. Chem. C* **2013**, *117*, 25756−25760.

(12) Nyk, M.; Szeremeta, J.; Wawrzynczyk, D.; Samoc, M. Enhancement of Two-Photon Absorption Cross Section in CdSe Quantum Rods. *J. Phys. Chem. C* **2014**, *118*, 17914−17921.

(13) Schwich, T.; Cifuentes, M. P.; Gugger, P. A.; Samoc, M.; Humphrey, M. G. Electronic, Molecular Weight, Molecular Volume, and Financial Cost-Scaling and Comparison of Two-Photon Absorption Efficiency in Disparate Molecules (Organometallic Complexes for Nonlinear Optics. 48.) - A Response to "Comment on 'Organometallic Complexes for Nonlinear Optics. 45. Dispersion of the Third-Order Nonlinear Optical Properties of Triphenylamine-Cored Alkynylruthenium Dendrimers.' Increasing the Nonlinear Response by Two Orders of Magnitude". *Adv. Mater.* **2011**, *23*, 1433−1435.

(14) Zelewski, S. J.; Nawrot, K. C.; Zak, A.; Gladysiewicz, M.; Nyk, M.; Kudrawiec, R. Exciton Binding Energy of Two-Dimensional Highly Luminescent Colloidal Nanostructures Determined from Combined Optical and Photoacoustic Spectroscopies. *J. Phys. Chem. Lett.* **2019**, *10*, 3459−3464.

(15) Vlaskin, V. A.; Janssen, N.; van Rijssel, J.; Beaulac, R.; Gamelin, D. R. Tunable Dual Emission in Doped Semiconductor Nanocrystals. *Nano Lett.* **2010**, *10*, 3670−3674.

(16) Tung, H. T.; Van Thuan, D.; Kiat, J. H.; Phuc, D. H. Ag^+ ion doped on the CdSe quantum dots for quantum-dot-sensitized solar cells' application. *Appl. Phys. A: Mater. Sci. Process.* **2019**, *125*, 505.

(17) Sharma, A.; Sharma, M.; Gungor, K.; Olutas, M.; Dede, D.; Demir, H. V. Near-Infrared-Emitting Five-Monolayer Thick Copper-Doped CdSe Nanoplatelets. *Adv. Opt. Mater.* **2019**, *7*, 1900831.

(18) Sharma, M.; Gungor, K.; Yeltik, A.; Olutas, M.; Guzelturk, B.; Kelestemur, Y.; Erdem, T.; Delikanli, S.; McBride, J. R.; Demir, H. V. Near-Unity Emitting Copper-Doped Colloidal Semiconductor Quantum Wells for Luminescent Solar Concentrators. *Adv. Mater.* **2017**, *29*, 1700821.

(19) Sharma, M.; Olutas, M.; Yeltik, A.; Kelestemur, Y.; Sharma, A.; Delikanli, S.; Guzelturk, B.; Gungor, K.; McBride, J. R.; Demir, H. V. Understanding the Journey of Dopant Copper Ions in Atomically Flat Colloidal Nanocrystals of CdSe Nanoplatelets Using Partial Cation Exchange Reactions. *Chem. Mater.* **2018**, *30*, 3265−3275.

(20) Liu, B.; Sharma, M.; Yu, J.; Shendre, S.; Hettiarachchi, C.; Sharma, A.; Yeltik, A.; Wang, L.; Sun, H.; Dang, C.; Demir, H. V. Light-Emitting Diodes with Cu-Doped Colloidal Quantum Wells: From Ultrapure Green, Tunable Dual-Emission to White Light. *Small* **2019**, *15*, 1901983.

(21) Jia-Jin, Z.; Gui-Lan, Z.; Yang-Xue, G.; Xiao-Yan, W.; Wen-Ju, C.; Xiao-Song, Z.; Yu-Lin, H. Two-Photon Absorption Properties of Mn-Doped ZnS Quantum Dots. *Chin. Phys. Lett.* **2006**, *23*, 3097−3100.

(22) de Mello, J. C.; Wittmann, H. F.; Friend, R. H. An improved experimental determination of external photoluminescence quantum efficiency. *Adv. Mater.* **1997**, *9*, 230−232.

(23) Dufour, M.; Izquierdo, E.; Livache, C.; Martinez, B.; Silly, M. G.; Pons, T.; Lhuillier, E.; Delerue, C.; Ithurria, S. Doping as a Strategy to Tune Color of 2D Colloidal Nanoplatelets. *ACS Appl. Mater. Interfaces* **2019**, *11*, 10128−10134.

(24) Khan, A. H.; Pinchetti, V.; Tanghe, I.; Dang, Z.; Martín-García, B.; Hens, Z.; Van Thourhout, D.; Geiregat, P.; Brovelli, S.; Moreels, I. Tunable and Efficient Red to Near-Infrared Photoluminescence by Synergistic Exploitation of Core and Surface Silver Doping of CdSe Nanoplatelets. *Chem. Mater.* **2019**, *31*, 1450−1459.

(25) Najafi, A.; Sharma, M.; Delikanli, S.; Bhattacharya, A.; Murphy, J. R.; Pientka, J.; Sharma, A.; Quinn, A. P.; Erdem, O.; Kattel, S.; Kelestemur, Y.; Kovalenko, M. V.; Rice, W. D.; Demir, H. V.; Petrou, A. Light-Induced Paramagnetism in Colloidal Ag^+-Doped CdSe Nanoplatelets. *J. Phys. Chem. Lett.* **2021**, *12*, 2892−2899.

(26) Nelson, H. D.; Hinterding, S. O. M.; Fainblat, R.; Creutz, S. E.; Li, X.; Gamelin, D. R. Mid-Gap States and Normal vs Inverted Bonding in Luminescent Cu+- and Ag+-Doped CdSe Nanocrystals. *J. Am. Chem. Soc.* **2017**, *139*, 6411−6421.

(27) Samoc, M.; Morrall, J. P.; Dalton, G. T.; Cifuentes, M. P.; Humphrey, M. G. Two-photon and three-photon absorption in an organometallic dendrimer. *Angew. Chem., Int. Ed.* **2007**, *46*, 731−733.

(28) Banyai, L.; Hu, Y. Z.; Lindberg, M.; Koch, S. W. Third-order optical nonlinearities in semiconductor microstructures. *Phys. Rev. B* **1988**, *38*, 8142−8153.

(29) Meulenberg, R. W.; Lee, J. R. I.; Wolcott, A.; Zhang, J. Z.; Terminello, L. J.; van Buuren, T. Determination of the Exciton Binding Energy in CdSe Quantum Dots. *ACS Nano* **2009**, *3*, 325−330.

(30) Xing, G.; Ji, W.; Zheng, Y.; Ying, J. Y. Two- and three-photon absorption of semiconductor quantum dots in the vicinity of half of lowest exciton energy. *Appl. Phys. Lett.* **2008**, *93*, 241114.

https://doi.org/10.1021/acsphotonics.1c01456
ACS Photonics 2022, 9, 256−267

(31) Li, J.; Zhang, S.; Dong, H.; Yuan, X.; Jiang, X.; Wang, J.; Zhang, L. Two-photon absorption and emission in CsPb(Br/I)3cesium lead halide perovskite quantum dots. *CrystEngComm* **2016**, *18*, 7945−7949.
(32) Papadakis, I.; Bouza, Z.; Couris, S.; Mouselimis, V.; Bourlinos, A. B. Dramatic Enhancement of the Nonlinear Optical Response of Hydrogenated Fluorographene: The Effect of Midgap States. *J. Phys. Chem. C* **2018**, *122*, 25573−25579.
(33) Li, T.; Dagenais, M. Non-resonant below-bandgap two-photon absorption in quantum dot solar cells. *Appl. Phys. Lett.* **2015**, *106*, 171101.
(34) Balu, M.; Padilha, L. A.; Hagan, D. J.; Van Stryland, E. W.; Yao, S.; Belfield, K.; Zheng, S.; Barlow, S.; Marder, S. Broadband Z-scan characterization using a high-spectral-irradiance, high-quality supercontinuum. *J. Opt. Soc. Am. B* **2008**, *25*, 159−165.
(35) Benjamin, E.; Yallapragada, V. J.; Amgar, D.; Yang, G.; Tenne, R.; Oron, D. Temperature Dependence of Excitonic and Biexcitonic Decay Rates in Colloidal Nanoplatelets by Time-Gated Photon Correlation. *J. Phys. Chem. Lett.* **2020**, *11*, 6513−6518.
(36) Rabouw, F. T.; van der Bok, J. C.; Spinicelli, P.; Mahler, B.; Nasilowski, M.; Pedetti, S.; Dubertret, B.; Vanmaekelbergh, D. Temporary Charge Carrier Separation Dominates the Photoluminescence Decay Dynamics of Colloidal CdSe Nanoplatelets. *Nano Lett.* **2016**, *16*, 2047−2053.
(37) Kunneman, L. T.; Schins, J. M.; Pedetti, S.; Heuclin, H.; Grozema, F. C.; Houtepen, A. J.; Dubertret, B.; Siebbeles, L. D. A. Nature and Decay Pathways of Photoexcited States in CdSe and CdSe/CdS Nanoplatelets. *Nano Lett.* **2014**, *14*, 7039−7045.
(38) Galland, C.; Ghosh, Y.; Steinbrück, A.; Sykora, M.; Hollingsworth, J. A.; Klimov, V. I.; Htoon, H. Two types of luminescence blinking revealed by spectroelectrochemistry of single quantum dots. *Nature* **2011**, *479*, 203−207.
(39) Ye, M.; Searson, P. C. Blinking in quantum dots: The origin of the grey state and power law statistics. *Phys. Rev. B* **2011**, *84*, 125317.
(40) Efros, A. L.; Nesbitt, D. J. Origin and control of blinking in quantum dots. *Nat. Nanotechnol.* **2016**, *11*, 661−671.
(41) Cichy, B.; Rich, R.; Olejniczak, A.; Gryczynski, Z.; Strek, W. Two blinking mechanisms in highly confined $AgInS_2$ and $AgInS_2$/ZnS quantum dots evaluated by single particle spectroscopy. *Nanoscale* **2016**, *8*, 4151−4159.
(42) Ayari, S.; Quick, M. T.; Owschimikow, N.; Christodoulou, S.; Bertrand, G. H. V.; Artemyev, M.; Moreels, I.; Woggon, U.; Jaziri, S.; Achtstein, A. W. Tuning trion binding energy and oscillator strength in a laterally finite 2D system: CdSe nanoplatelets as a model system for trion properties. *Nanoscale* **2020**, *12*, 14448−14458.
(43) Shornikova, E. V.; Yakovlev, D. R.; Biadala, L.; Crooker, S. A.; Belykh, V. V.; Kochiev, M. V.; Kuntzmann, A.; Nasilowski, M.; Dubertret, B.; Bayer, M. Negatively Charged Excitons in CdSe Nanoplatelets. *Nano Lett.* **2020**, *20*, 1370−1377.
(44) Yuan, G.; Gómez, D. E.; Kirkwood, N.; Boldt, K.; Mulvaney, P. Two Mechanisms Determine Quantum Dot Blinking. *ACS Nano* **2018**, *12*, 3397−3405.
(45) Li, B.; Zhang, G.; Wang, Z.; Li, Z.; Chen, R.; Qin, C.; Gao, Y.; Xiao, L.; Jia, S. Suppressing the Fluorescence Blinking of Single Quantum Dots Encased in N-type Semiconductor Nanoparticles. *Sci. Rep.* **2016**, *6*, 32662.
(46) Frantsuzov, P.; Kuno, M.; Jankó, B.; Marcus, R. A. Universal emission intermittency in quantum dots, nanorods and nanowires. *Nat. Phys.* **2008**, *4*, 519−522.
(47) Morgan, D.; Kelley, D. F. Role of Surface States in Silver-Doped CdSe and CdSe/CdS Quantum Dots. *J. Phys. Chem. C* **2018**, *122*, 10627−10636.
(48) Sahu, A.; Kang, M. S.; Kompch, A.; Notthoff, C.; Wills, A. W.; Deng, D.; Winterer, M.; Frisbie, C. D.; Norris, D. J. Electronic Impurity Doping in CdSe Nanocrystals. *Nano Lett.* **2012**, *12*, 2587−2594.

https://doi.org/10.1021/acsphotonics.1c01456
ACS Photonics 2022, 9, 256−267